

https://dspace.org/

Effects of selected cathode materials on a magnetically enhanced vacuum arc thruster

Tristan Rencken; Philippe Ferrer

PERGAMON-ELSEVIER SCIENCE LTD
https://hdl.handle.net/10539/40889
WOS

Downloaded from a DSpace repository. https://dspace.org/

Acta Astronautica 220 (2024) 321–329

Contents lists available at ScienceDirect

Acta Astronautica

journal homepage: www.elsevier.com/locate/actaastro

Effects of selected cathode materials on a magnetically enhanced vacuum arc thruster

T. Rencken [a], P. Ferrer [b,*]

[a] School of Mechanical, Industrial and Aeronautical Engineering, University of the Witwatersrand, Johannesburg, 2001, South Africa
[b] School of Physics, Mandelstam Institute for Theoretical Physics, University of the Witwatersrand, Johannesburg, 2001, South Africa

ARTICLE INFO

Keywords:
Electric propulsion
Vacuum arc thruster
Magnetically enhanced
Cubesat propulsion system

ABSTRACT

We discuss the effects of the ion distribution of a magnetically-enhanced Vacuum Arc Thruster using different cathode materials (Fe, Al, Cu) and magnetic field strengths. We develop a formalism, which is based on physical and geometric ideas, that describes the data for the inclusion of a magnetic field better than previous models ($R^2 > 0.89$ for worst case). Our tests were performed on a Vacuum Arc Thruster with 270 A discharge current and an average pulse length of 3.5 ms. The magnetic field generator, driven by a separate capacitive discharge circuit, produced field strengths ranging from 0 to 250 mT along the thruster's centerline. We obtained the thrust correction factor and theoretical thrust from our measurements. It was found that application of magnetic fields increased ion density and axial momentum along the plasma plume's centerline. At higher magnetic field strengths (~250 mT) the thrust factor decreased across all materials. For our electrodes, the inclusion of a protruding magnetic nozzle was seen to cancel the benefits arising from beam collimation due to the magnetic field. The iron electrode performed best, which may be due to its ferromagnetic nature.

1. Introduction

Miniaturized propulsion modules are becoming increasingly popular for orbital maneuvers and controlled de-orbiting [1,2]. One available option for compact electric propulsion is a Vacuum Arc Thruster (VAT), where work is done on small satellite integration [3]. A VAT propulsion system is one that uses an arc discharge between an anode and cathode to produce thrust by creating a high-density plasma on the surface of the cathode. The expansion of this plasma contains ions that can travel at velocities between 10 and 20 km/s [4]. The thruster is versatile and allows for different incarnations. Many aspects are areas of active research, such as the support circuitry, where new ways of storage are discussed [5], and physical aspects, which address efficiency and reliability (more than 10^7 pulses) with a magnetic coil attached [6,7].

An incarnation of the VAT is the Magnetically-Enhanced Vacuum Arc Thruster (MEVAT). The MEVAT uses as an added feature an external axial magnetic field, generated by a coil around the cathode, to collimate the plasma produced on the cathode surface [8]. This application has several benefits, including increased plasma collimation, which reduces surface contamination of spacecraft and increases ion velocity and current. Some performance improvements were recorded, such as a doubling of the thrust-to-weight ratio, resulting in a thrust generation of 21 μN at 2.7 W of average arc power and a 4 % thrust efficiency [9]. MEVATs are also simple and compact, making them suitable for use in small spacecraft. Additionally, the application of a magnetic field to the VAT leads to better cathode erosion rates and cathode spot rotation, which results in the homogeneous erosion critical for thruster lifecycle performance. A two-stage system was studied by Zolotukhin et al. [10], which was capable of reaching very high thrusts and efficiencies.

MEVATs have been the subject of numerous studies investigating the effects of the magnetic field on plasma jet dynamics, thrust performance, and potential applications in space missions. Xia et al. conducted an experimental demonstration of micropropulsion using a magnetic VAT for CubeSat attitude control and found that the magnetic field helped to control the plasma jet's performance, and that the magnetic nozzle was able to increase the thrust and specific impulse of the thruster [11]. Wang et al. conducted an experimental study of the plasma parameters and thrust performance of a magnetic VAT with a helicon antenna and found that the magnetic field can affect plasma density and temperature, which in turn affects thrust performance [12].

Another theoretical study by Li et al. investigated the use of a pulsed power supply to generate high-velocity plasma jets in a vacuum arc

* Corresponding authorSchool of Physics, University of the Witwatersrand, Johannesburg, South Africa.
E-mail address: Philippe.ferrer@wits.ac.za (P. Ferrer).

https://doi.org/10.1016/j.actaastro.2024.04.038
Received 14 November 2023; Received in revised form 15 April 2024; Accepted 25 April 2024
Available online 30 April 2024
0094-5765/© 2024 IAA. Published by Elsevier Ltd. All rights reserved.

thruster. They found that the pulsed power supply was able to generate plasma jets with higher velocity and density compared to a continuous power supply [13]. Baranov et al. used numerical simulations to investigate the effect of magnetic field configuration on the performance of a magnetic VAT and found that optimizing the magnetic field can significantly increase specific impulse and thrust efficiency [14]. Takahashi et al. used numerical simulations to study the performance of a magnetic VAT with a magnetic nozzle and also found that the magnetic field can significantly affect flow dynamics and thrust performance [15].

However, it was seen that different cathode materials can affect performance parameters [4]. A study where the same MEVAT is used with different cathode materials could therefore be of importance when finalizing cathode choice. The primary aim and novelty of this study was to develop a more physically intuitive formalism for the ion current distribution, and to study a magnetically enhanced VAT for different cathode materials. We chose Fe, Cu and Al electrodes for the investigation, since we were less interested in performance than in how the performance would be affected by the inclusion of a magnetic nozzle and field.

It was seen that the magnetic field collimated the beam for all cases, but that the momentum lost to the nozzle largely cancelled the benefits. Further, the iron electrode performed best from the "bare" case (without coil attached) to the best case, at B = 150 mT.

In section 2 we develop the formalism we will used to fit to the ion current distribution data, and in Section 3 we introduce the experimental equipment and procedure. Sections 4 and 5 deal with results, discussion and conclusion.

2. Ion current and plasma shadowing formalism

2.1. Ion current distribution

We next discuss the formulation of a semi empirical model which will assist us in interpreting our experimental data. We will use results from previous authors [4,16] and extend them to describe the current case.

Cathode spots erode in the form of macro particles, droplets and ions. Macroparticles are typically emitted at shallow angles to the cathode's normal axis and at low average velocities (400 m/s) [4,17].

Our primary interest lies in the ion component, which for the current levels of interest to us was seen to be a constant fraction (denoted f_i) of the discharge current in previous experiments [18]. It was also seen that the plasma plume created by the cathode spots contains a number of differently charged ion species which equilibrate to a final charge state distribution (CSD) at some point, as the plasma plume expands and cools, and the charge transfer interaction cross-section is reduced.

The iron current density in the plume expanding from the infinitesimal area dA located at the cathode spot has been described empirically using cosine and exponential distributions [17]. In what follows, we will concentrate on the exponential distribution since it has a free parameter, k, describing its spread while the cosine distribution does not allow for such a variation. The spread of the ion current distribution will be seen to vary with application of a magnetic field.

The distributions are symmetric along the azimuthal direction and describe the ion current distribution in terms of polar angle Φ and the distance l from dA, the location of the cathode spot. The amplitude κ of the distribution is proportional to the ion current density at the cathode j_{ic}, inversely proportional to the square of the distance from dA, and factors related to the spread, k. It is given by

$$j_{ip}(l,\varphi) = \kappa \bullet dA_1 \bullet \exp\frac{\left(-[2\pi(1-\cos\varphi)]^2/k^2\right)}{l^2} \tag{1}$$

with $\kappa = \frac{2j_{ic}}{\sqrt{\pi}k\left(\mathrm{erf}\left(\frac{2\pi}{k}\right)\right)}$.

For a cathode of finite size, dA has to be integrated over to yield the ion current density $J_{ip}(R,\ \Phi)$. In many cases the cathode area is circular with radius r'_c and for such a geometry the distribution is

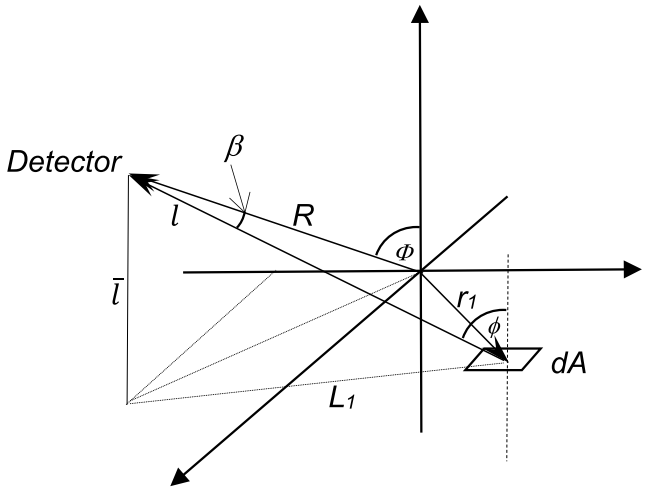


Fig. 1. Geometry of ion current distribution due to a finite size cathode.

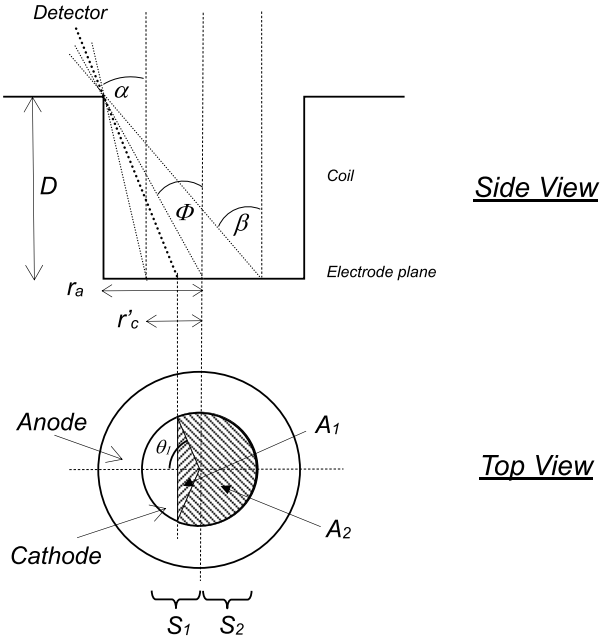


Fig. 2. Geometric representation of coil shadowing. The ion current on the detector is reduced due to the smaller ion source area (A_1 and A_2), see text.

$$J_{ip}(R,\Phi) = \kappa \int_0^{2\pi} d\theta_1 \int_0^{r'_c} dr_1 I_D \tag{2}$$

and

$$I_{D=r_1} \frac{\exp\left(-\left[\frac{2\pi}{k}\left(1-\frac{\bar{l}}{\sqrt{\bar{l}^2+L_1{}^2}}\right)\right]^2\right)}{\bar{l}^2+L_1{}^2} cos\,\beta,$$

where the angle Φ is now taken from the center of the cathode, and θ_1 is the azimuthal angle to r_1, the distance from the cathode center to dA. The dimensions of interest are indicated in Fig. 1.

In the limit as R (the distance from the cathode center to the ion current detector) is much larger than r'_c, equation (2) reduces to equation (1).

2.2. Coil shadowing

In a common arrangement of a VAT, the cathode and the anode are coplanar, with the circular cathode being in the center surrounded by an anode annulus, and separated by a thin insulator. If a magnetic coil is introduced to apply a magnetic field perpendicular to the electrodes' surface, it may extrude a distance D past the plane of the electrodes, see Fig. 2. Such a coil now forms a material obstruction for any ions propagating in a direction larger than the angle β (Fig. 2). More than that, at any azimuthal angle, the cathode surface appears partially obstructed by the coil, or "shadowed", if viewed between the angle α and β and therefore, since it is the source of the ion current, this shadowing will reduce the ion flux along this angle interval in proportion to the amount of area that is shadowed.

The shadow which reduces the cathode area takes the form of a circular section proportional to the coil radius. Although an integral describing this can be straightforwardly constructed, in what follows we shall assume the cathode area to be cut by a straight line shadow (see Fig. 2, top view) as an approximation valid when the coil radius is larger than the cathode radius.

The shadow can be described in terms of the parameters of Fig. 2: only areas A1 and A2 will contribute to the ion current flux. The cathode area contributing to the ion current (active region) can be split into the triangular region A1 and the circular arc section A2.

The angle θ_1 is related to the angle Φ straightforwardly through the relation

$cos\,\theta_1 = \frac{r_a - D tan\Phi}{r_c'}$ for $\alpha < \Phi < \beta$,Where the shadowing effect is assumed to take effect between the angles α and β.

To obtain the ion current which is reduced by the "shadow", integration takes place over the active region, areas A1 and A2. The ion current distribution is then given by

$$J^{S_1}(R,\Phi) = 2\kappa\left[\int_{\theta_1}^{\pi} d\theta \int_0^{r_c'} dr_1 I_D + \int_0^{\theta_1} d\theta \int_0^{r_c' \cos(\theta_1)\sec(\theta)} dr_1 I_D\right] \quad (3)$$

for the region denoted S_1, for $\theta_1 < \frac{\pi}{2}$, which is the first half circle of the circular cathode that is shadowed, as Φ increases from α to $\frac{\alpha+\beta}{2}$, see Fig. 2. The shadowed region then moves on to partially cover the second half circle S_2, and the ion current is described at these angles Φ between $\frac{\alpha+\beta}{2}$ to β by S_2, for which $\theta_1 > \frac{\pi}{2}$,

$$J^{S_2}(R,\Phi) = 2\kappa\left[\int_{\theta_1}^{\pi} d\theta \int_0^{r_c'} dr_1 I_D - \int_{\pi}^{\theta_1} d\theta \int_0^{r_c' |\cos(\theta_1)\sec(\theta)|} dr_1 I_D\right] \quad (4)$$

In the un-shadowed region, where Φ is between α and zero, the distribution of equation (2) is used.

Assumptions made for this description are that the ion flux to be measured originates mainly from a region close to the electrode plane; and the distance R is large compared to the effective cathode radius.

2.3. Effective cathode radius

The exponential ion current distribution, equation (1), was originally used in a situation where the anode was directly above a circular cathode plane [19]. Further, it was introduced as an improvement over the cosine distribution, since it explained an ion flux at angles even below the cathode plane, which must have been scattered from the plasma discharge region. The plasma density remains quite high in a region about 5 mm above the electrode plane, and can extend to >2 cm along it [8], for arc currents around 200 A. In the inter-electrode gap the plasma density is of the order 10^{21} m^{-3} and inelastic collisions are rare [20], while the electron mean free path is smaller than the jet plume radius, leading to ion-electron elastic collisions, and scattering. It is therefore believed that the plasma jet region contributes to the angular ion current distribution.

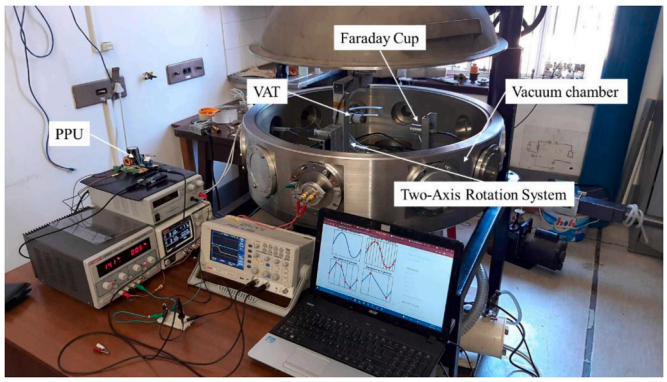


Fig. 3. Stainless steel vacuum chamber used for vacuum arc thruster testing with automated real-time data collection.

The geometry used in this research does not reflect the geometry of [19]. In our case, the anode is co-planar with the cathode, so the discharge plasma is confined more along the electrode plane, extending from the centered circular cathode outwards to the anode annulus. We take the plasma discharge region to act as a secondary "source" of ions, effectively increasing the ion source region from "only" the material cathode, to regions further away from the center, above the anode. The anode potential may even assist in accelerating these ions away from the electrode plane.

We therefore introduce the concept of an "effective" cathode radius, r'_c, which is larger than the material cathode and takes into account ions originating from the entire discharge region from anode to cathode and contributing to the ion current flux. We assume that these secondary (scattered) ions originate from quite close to the electrode plane, and that they have a similar emission rate throughout the discharge region. This last assumption can likely be refined to non-constant ion emission rates from the plume.

We determined from the goodness of fit to the data that this formalism of the effective cathode radius shadowed region, which is based on geometric and physical considerations, describes the measured ion current distribution better than a variation of k in equation (2), alone.

We will use curves fitted to data using the formalism of the preceding section in order to evaluate the thrust factor C_T as described in Ref. [4], and calculate the theoretical thrust.

2.4. Thrust correction factor and thrust

According to Ref. [4], the ion distribution within the plasma plume can represent the thrust produced by the VAT sufficiently well on its own. The thrust correction factor C_T provides a measure of the thrust that can be obtained from an ion current distribution. This is done straightforwardly by converting the ion current flux, equation (2), into a momentum flux by using the average charge state of the ions and their mass. The momentum components perpendicularly away from the electrode plane are integrated over, to obtain the total thrust acting on the VAT. In case of material obstructions like coils, the un-intercepted ion flux is integrated over, while the momentum contribution of ions colliding with the material obstruction is ignored, since they provide no net thrust.

The thrust correction factor C_T is used in the description of the net thrust T produced by a VAT,

$$T = \frac{M_i f_i J_{arc} u_i}{e\langle Z\rangle} C_T \quad (5)$$

where M_i, f_i, J_{arc} and u_i are the ion mass, ion current to arc current ratio, total arc current and average ion velocity of the ion species i, respectively.

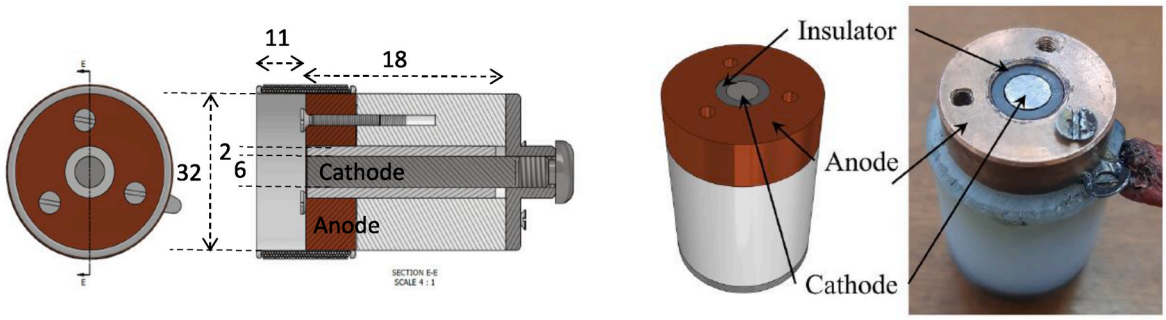


Fig. 4. Selected vacuum arc thruster coaxial design (left) with inner cathode rod, ceramic alumina insulator and outer anode. Ultra-high-molecular-weight polyethylene housing with anode attached to positive terminal of the pulse power unit circuit. The magnetic coil is placed around the anode. Design (right) and product. All units are in millimetres.

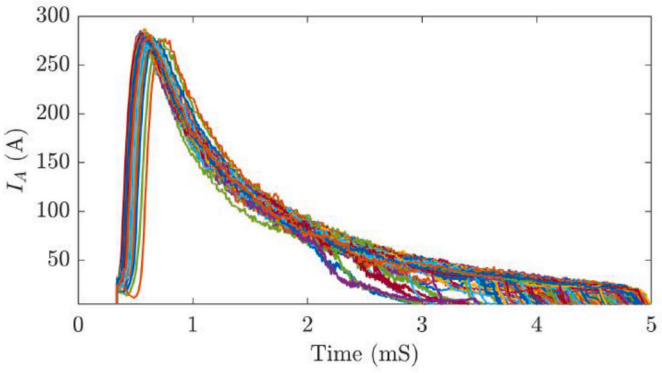


Fig. 5. Sample pulse length study of 1000 pulses for Al cathode vacuum arc thruster with an average pulse length of $t_p = 4.5 \pm 0.3$ ms. Pulse repetition was at a low frequency, around 0.2 Hz.

3. Experimental procedure

The ion current density distribution (ICDD) data of a constructed VAT was collected in a stainless-steel vacuum chamber (see Fig. 3.) performed at vacuum levels between 1.3 and 6.6 $\times$ 10^{-4} Pa.

The VAT was designed and built in-house as seen in Fig. 4, where the "bare" VAT contained no coil, and the coil was added in subsequent experiments requiring a magnetic field.

Three different materials (Al, Cu, Fe) were selected for the central cathode of radius $r_c = 3$ mm and length 18 mm, insulator spacing of 2 mm, and $r_a = 16$ mm, all with error ($\pm$ 0.1 mm).

Copper was chosen for the anode material throughout. The experiments were conducted without cathode feeding, with the cathode being replaced manually at intervals. The VAT was operated at a low rate of 0.2–0.3 Hz, since optimizing performance was not the primary objective, but measuring the ion current distribution was. A graphite layer was applied to the insulator before first use to initiate discharge.

A circuit for the pulsed power unit (PPU) was constructed similar to the one used in [22]. The efficiency of the PPU was a secondary concern to its reliability and was not evaluated.

The PPU was used to control the arc current by varying the charging duration, which allowed for a pulse range of 3–5 ms to be consistently produced during testing. Fig. 5 shows a sample pulse testing we used to ensure stability.

The circuit tuning process was successful in achieving a consistent maximum arc current range between 260 and 280 A for all three cathode materials.

Inclusion of the coil changed the VAT as seen in Fig. 6.

The coil consisted of enamelled copper wire of 0.5 mm diameter thickness and 100 loops. The current through the wire was adjusted so as to give the desired field strength, and found from a MATLAB simulation of such a system, see Fig. 7. It was further measured by the voltage induced in a search coil, before testing. The magnetic field was synchronised with the arc pulses. Incorrect timing could introduce firing problems as was pointed out by Zolotukhin et al. [21], and permanent magnets have been suggested.

A Faraday cup probe was used to measure the ion current density at selected angles relative to the electrode surface, by using a Two-Axis Rotation System (TARS) (Fig. 8).

The Ion Current Density Distribution was measured using a Faraday cup (Fig. 9) placed in the near-field region of the plasma plume (separated during measurement by 15 $mm\pm$ 2), capturing charged particles,

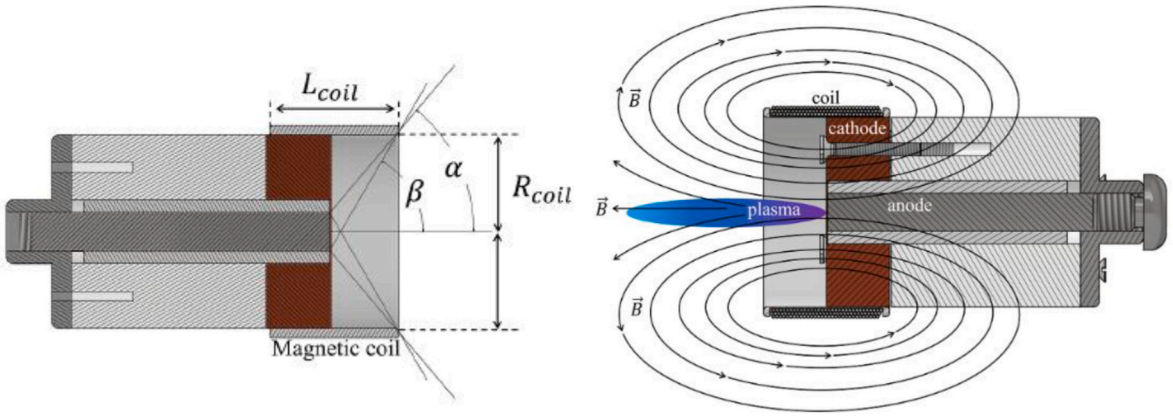


Fig. 6. Thruster geometries of magnetic coil positioning demonstrating the plasma shielding angle. α and β represent the maximum and minimum sight angles for the variation in arc discharge along the surface of the cathode.(Right) Magnetic field produced by coil, which collimates the emerging plasma beam.

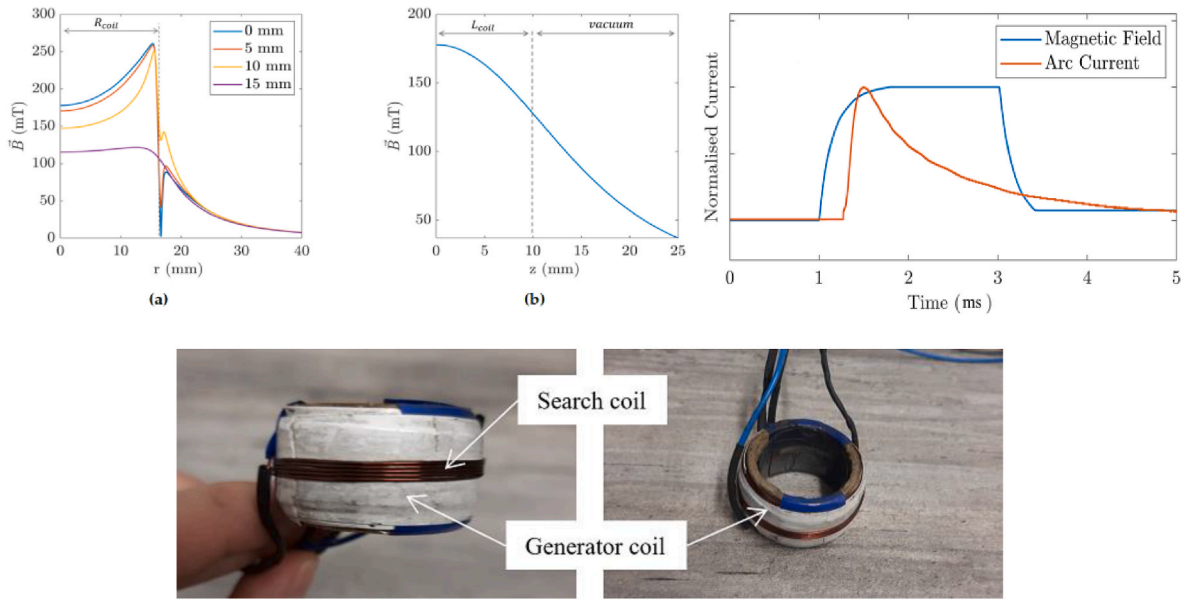


Fig. 7. (Top left) Initial MATLAB simulated magnetic field results for coil design (a) Radial magnetic field strength (b) Magnetic field strength along the center axis (cathode at 0 mm). (Top right) timing sequence of magnetic field relative to arc current. (Below) search coil for measurement of magnetic field strength.

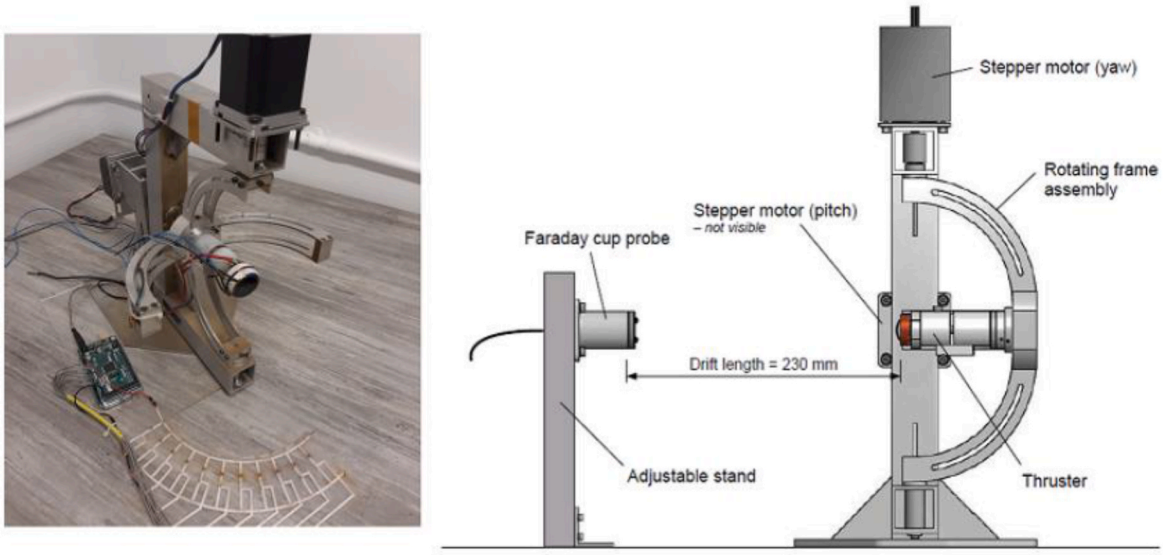


Fig. 8. Two-Axis Rotation System with stepper motor for accurate angle variation. (left) Two-Axis Rotation System with laser optical alignment system used to ensure accurate angle positioning of vacuum arc thruster during testing [22].

and measuring the average peak ion voltage. Radial and axial measurements were taken and compared favourably to expectations.

The average peak arc current (the discharge current through the plasma) was measured for every thruster configuration (bare, coil and B $\neq$ 0). The voltage reading in the Faraday cup probe was noted and related to the ion current via a shunt resistor. This reading was taken at an angle from 0° to 90° relative to the electrode surface, in increments of 9°($\pm$1°), during close to 400 pulses per increment. The signals were captured using a Pico Technology Pico scope 5443D MSO with a 125 MS/s sampling rate, which produced 625,000 data points per channel. All signals were captured for each VAT pulse, which was triggered by the inductor pulse (see Fig. 10).

From each test, 150 successful discharges were kept and filtered to clean the signal from the stochastic nature of the discharge. From this the average ion current readings were obtained for every configuration, at every angle.

4. Results

The ion current data collected as described in Section 3 was modelled using the formalism introduced in Section 2, for the different cathode materials (Fe, Cu, Al), and the following thruster configurations: 1) a VAT as depicted in Figs. 4 and 2) a VAT with coil attached (B = 0 T) (Figs. 6) and 3) a VAT with coil producing a magnetic field, $B = 150$ mT and $B = 250$ mT.

We computed the thrust correction factor, and the expected thrust for each configuration, according to Section 2.4 (see Table 1).

The tests were performed using identical circuit parameters, arc currents, and sample sizes. The ion current distributions were normalised to their relative peak arc current values (see Table 2). The error introduced for converting the voltage reading from the Faraday cup (see Fig. 9) to a value for the ion current from the shunt resistor proved too large, so we assumed a constant ion to arc fraction for the readings and

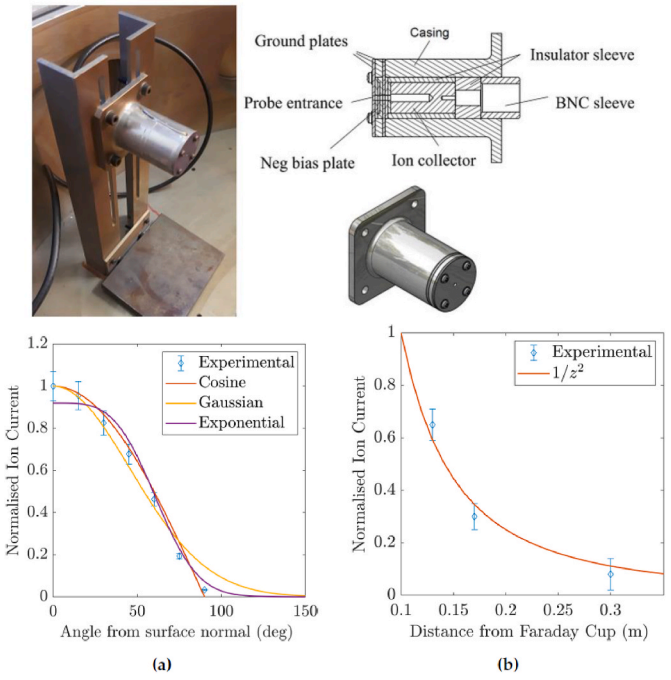


Fig. 9. Faraday cup set up inside the vacuum chamber and schematic. (Below) Faraday cup calibration (a) angular and (b) as a function of distance.

included this error in the evaluation of the thrust. Each measured distribution for the bare VAT was fitted to a curve as described by equation (2) with r_c and k varying.

The results are shown in Fig. 11 and the fitting parameters, as well as experimental parameters, displayed in Table 2.

Equation (2) describes the ion current distributions fairly well as can be seen from the R^2 test, displayed in Table 2.

Next, we analysed the results for a VAT including a coil attachment as described in Section 3. The ion current distributions were again normalised to their relative peak discharge current values (see Table 3). We assumed that the presence of the coil with $B = 0$ mT would not have any significant effect on the spread k of the ion current distribution, since there is no compelling physical reason for the spread to change due to the presence of an obstacle (coil) a "long" distance away.

We therefore took the k values for each electrode that were obtained for the curves fitted to VAT without coils, Table 2. The measured distribution was then fitted to the curves as outlined by equations (2)–(4), by keeping k constant and varying r'_c for the best fit. We subsequently tested that assumption varying k after we had obtained a best-fit r'_c. This did not yield any better fit within the error of k.

The effective cathode radius r'_c for the best fit was $r'_c = 16$ mm in each case. This is significant since it indicates that the entire cathode and anode surface may have been active in the production of the ion current distribution – the cathode through cathode spots, and the anode due to scattering throughout the plasma discharge found above its surface. This statement requires further experimental verification, but it may be plausible since the plasma density was shown to be quite high even at a distance of 2–3 cm from the center of the electrodes [4].

The data and fitted curves are given in Fig. 12.

The graph terminates at the data points ± 63°, since then the electrode plane is in complete shadow, and any ion current measurements would be a consequence of ions scattered well above it. The formalism outlined in Section 2.2 does not describe the scattered ion flux from such a region well. The results are summarized in Table 3.

Next, we analysed the results for a VAT including the coil inducing a magnetic field $B = 150$ mT as estimated in Section 2.

Table 2
Parameters fitted to the "bare" vacuum arc thruster, without coil attached.

	J_{arc} ($A \pm 5$)	r'_c ($mm \pm 1$)	k (± 0.2)	R^2	C_T (± 0.01)	*Thrust* ($N \pm 29\%$)
Fe	269	16	3.9	0.987	0.668	0.057
Al	277	16	3.9	0.975	0.668	0.076
Cu	274	16	3.8	0.975	0.674	0.065

The value of k for the three different electrodes is similar.

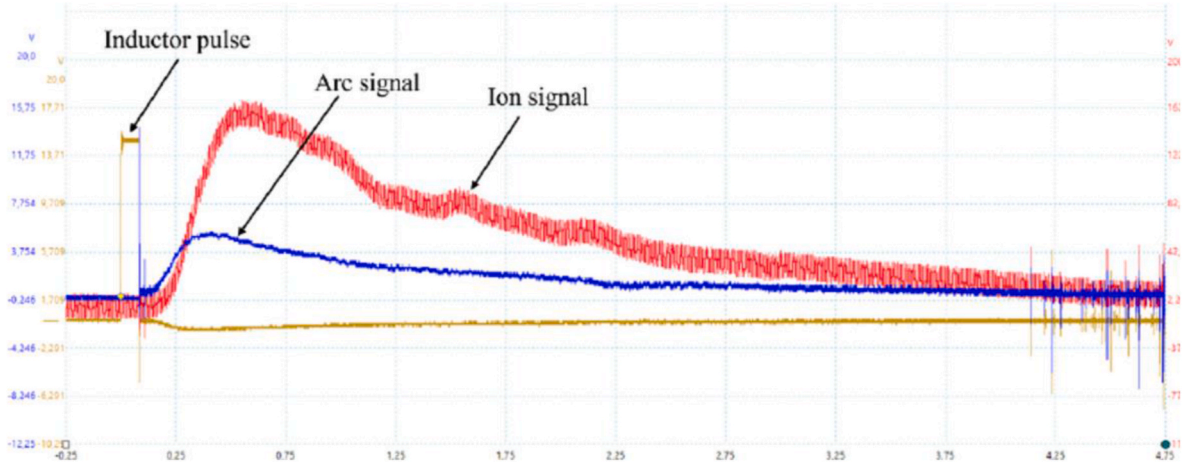


Fig. 10. Electrical signal as from a vacuum arc thruster pulse, as recorded by the Pico Scope. Shown is the inductor pulse, arc current and Faraday cup voltage.

Table 1
Properties of cathode material [23]:.Mass (AMU), ion velocity u, average charge of ions <Z>, density ρ(g/cm^3), electric conductivity σ(MS/m), melting point T_m (∘C), thermal conductivity λ_T(W/(m·K)).

Material	M_i *(AMU)*	u *(m/s)*	<*Z*> *(e/ion)*	ρ(g/cm^3)	σ(MS/m)	T_m (∘C)	λ_T(W/(m·K))
Cu	63.6	12,800	2.04	8.02	58.0	1084.62	401
Al	26.9	29,900	1.72	2.38	36.59	660.32	243
Fe	55.9	11,800	1.81	6.98	10.02	1538	80.2

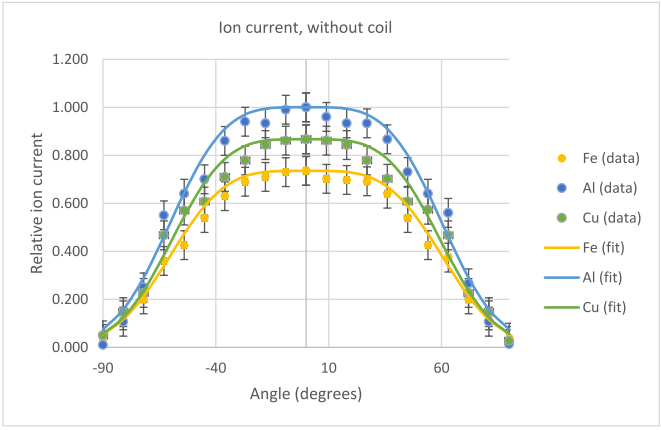


Fig. 11. Data and fitted curves for the angular ion current measurements of a "bare" vacuum arc thruster, for the Fe, Al and Cu electrodes.

Table 3
Parameters fitted to the vacuum arc thruster, with coil attached, magnetic field $B = 0$ mT.

	J_{arc} ($A \pm 5$)	r'_c ($mm \pm 1$)	k (± 0.2)	R^2	C_T (± 0.01)	*Thrust* ($N \pm 29\%$)
Fe	269	16	4.3	0.891	0.388	0.033
Al	277	16	3.9	0.915	0.412	0.047
Cu	274	16	4.1	0.894	0.399	0.039

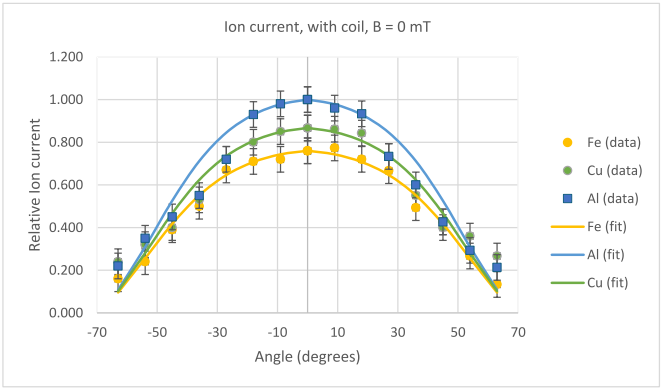


Fig. 12. Data and fitted curves for the angular ion current measurements of a vacuum arc thruster with coil, magnetic field $B = 0$ mT, for the Fe, Al and Cu electrodes.

Table 4
Parameters fitted to the vacuum arc thruster, with coil attached, magnetic field $B = 150$ mT.

	J_{arc} ($A \pm 5$)	r'_c ($mm \pm 1$)	k (± 0.2)	R^2	C_T (± 0.01)	*Thrust* ($N \pm 29\%$)
Fe	274	16	1.5	0.987	0.668	0.059
Al	280	16	2.2	0.993	0.572	0.066
Cu	279	16	2.0	0.961	0.598	0.059

It is worth noting that the peak ion-to-arc current ratio remained unchanged for all materials when the coil was attached. The ion current distributions were again normalised to their relative peak discharge current values (see Table 4). We assumed here that the presence of the magnetic field would have an effect on the spread k of the ion current distribution, since the magnetic field lines act to collimate the particles in the direction perpendicular to the electrode plane. The effect on the ion current distribution is to reduce the spread.

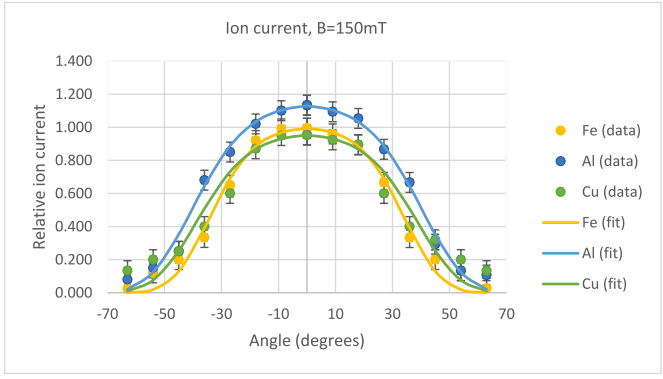


Fig. 13. Data and fitted curves for the angular ion current measurements of a vacuum arc thruster with coil, magnetic field $B = 150$ mT, for the Fe, Al and Cu electrodes. The Fe distribution is narrow and peaks above the Cu distribution.

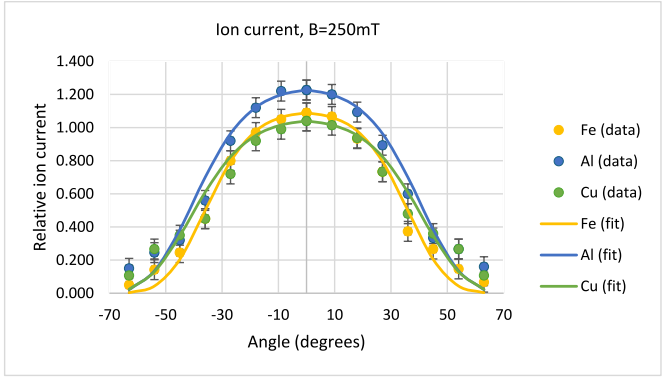


Fig. 14. Data and fitted curves for the angular ion current measurements of a vacuum arc thruster with coil, magnetic field $B = 250$ mT, for the Fe, Al and Cu electrodes.

Table 5
Parameters fitted to the vacuum arc thruster, with coil attached, magnetic field $B = 250$ mT.

	J_{arc} ($A \pm 5$)	r'_c ($mm \pm 1$)	k (± 0.2)	R^2	C_T (± 0.01)	*Thrust* ($N \pm 29\%$)
Fe	270	16	1.7	0.987	0.639	0.055
Al	277	16	2.2	0.980	0.573	0.065
Cu	279	16	2.3	0.971	0.560	0.055

We took the same r'_c values for each electrode as were obtained for the graph in Fig. 12, since we did not expect the effective cathode radius to change. The size of the plasma region, when a magnetic field is switched on, remains almost unchanged for distances of interest to us ($\sim r_a$) [24].

The measured distribution was then fitted again to the curves as outlined by equations (2)–(4) and varying k for the best fit. We subsequently tested that assumption again by varying r'_c after we had obtained a best-fit k, without finding a better fit within the error limits.

The data and fitted curves for the electrodes are given in Fig. 13, with results in Table 4.

The values of k for all curves have reduced from the un-magnetized case, see Table 3. Further the ions of the Fe electrode are more sharply peaked than for the Cu electrode, with the Fe maximum larger than the Cu maximum.

A similar procedure was followed for the case of $B = 250$ mT, with the results given by Fig. 14, and tabulated in Table 5.

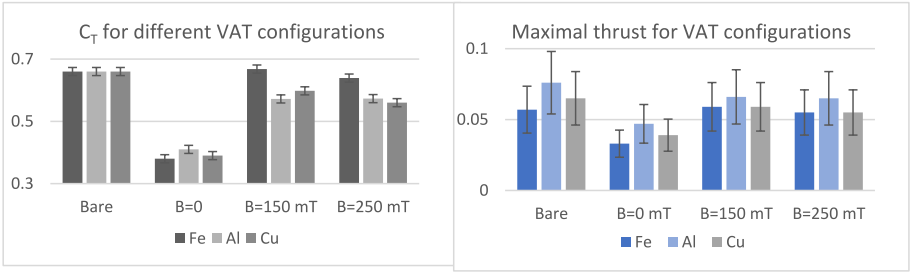


Fig. 15. The thrust correction factor (left) for the different electrodes at different magnetic fields, and the thrust (right) for the same configurations. The error for the thrust is large, making comparison difficult.

Again Fe is larger than Cu, but here the values of k have increased compared to the $B = 150$ mT case.

The magnetic field had an insignificant effect on peak arc current, which are similar findings as [9,24]. They reported that the most significant increase in thrust was observed at a magnetic field strength of 120 mT, with substantially lower values noted at either higher or lower magnetic fields. The lower thrust values were accompanied by a decrease in arc duration, and some with a lower overall arc energy.

5. Discussion

The framework we developed in Section 2 seems to fit the data well, with R^2 values in excess of 0.891. This lends some credence to the physical interpretation of the fitting procedure. The fit started deviating from the expectations at large angles, where ion scattering states are likely to dominate. The error range for C_T was obtained for the distributions by choosing the extreme values from the ion current measurements and fitting a curve to these extremum curves.

The thrust correction factor is influenced by the presence of the coil, and the focusing of the beam by the magnetic field. The presence of the coil nearly halves C_T and has a negative effect on thrust efficiency, see Fig. 15. The magnetic field restores the C_T almost to the level of the bare thruster (without coil) except for the Fe electrode at $B = 150$ mT, where C_T is slightly exceeded, see Table 4.

The theoretical thrust calculated from equation (5) indicates that, in our case, only the Fe electrode shows potential of exceeding the thrust of the bare VAT. It was however postulated that the Mach number of the ions could increase, for instance, by approximately 20%–28 % in the case of a Ti electrode [24] and this effect has not been included in the calculations. Looking at the thrust description, $T = \frac{M_i f_i J_d u_i}{e\langle Z\rangle} C_T$ the factors which are affected by application of an external magnetic field are f_i, u_i and C_T, at the same arc current. The highest thrust scenario at constant discharge energy is an increase of f_i from about 0.07 to 0.1, u_i has been postulated to be able to show a 28 % increase (for Ti ions) and C_T can go from about 0.67 for a bare thruster to 1 (collimated beam). This amounts to a maximal thrust increase of ~270 %. More realistically is that f_i is unaffected, the ion speed increase is around 25 % while C_T remains roughly constant, the coil shadowing being compensated by the plume focusing. A thrust increase of around 25 % is expected in this case. In our case, the computed error for the thrust is similar to the expected increase, so we cannot comment on it.

An increase in the discharge energy at magnetic fields between 0.05 mT and 0.2 mT was reported by [24], which could further increase the thrust. At constant discharge energy, addition of a magnetic field has an effect on the arc current duration (decreasing it) and the discharge voltage (raising it) [24]. Since the thrust is proportional to the ion current (and hence the arc current), a longer arc duration would favour both thrust and efficiency.

The Fe electrode shows improved behavior even compared to the other electrodes, in the presence of a magnetic field. The ferromagnetic nature of Fe will certainly have increased the magnetic field close to the cathode to values exceeding our estimates, and therefore a smaller external B field would be required to attain, say 150 mT close to the electrode surface.

The results of C_T and thrust are summarized in Fig. 15.

6. Conclusion

We derived a formalism in Section 2 based mainly of physical and geometrical considerations to deal with the ion current distribution of a vacuum arc thruster with the inclusion of a coil (or other material obstacles). We used the formalism to fit curves to data we measured from ion current distributions, and found the curves to fit the data well.

We studies three different electrode materials (Fe, Al, Cu) under varying conditions (no coil, coil, B = 0, 150 mT, 250 mT) and used our curve fitting formalism to derive a value for the thrust correction factor C_T, one measure of thruster efficiency. We found that the presence of the coil, even with the magnetic field switched on, has an overall detrimental effect for the electrodes we studied, reducing the thrust correction factor and hence the efficiency. Although a magnetic nozzle is generally accepted as improving vacuum arc thruster performance, in our study the presence of the coil seems to undo the benefits from the beam collimation. Thrust improvement must therefore rely on other factors, such as the change of the discharge electrical profile, and space charge effects for ion velocity increase.

The iron electrode performed better with coil and magnetic field active, but is likely to have had an increased magnetic field due to its ferromagnetic nature, hence inclusion of such material may improve performance.

Inclusion of a magnetic field will not guarantee an overall performance improvement of a satellite's mobility. An immediate concern is the large effect that the presence of a coil has in reducing thrust efficiency, by introducing a material barrier. Other improvements will not be very effective unless the material barrier is reduced. Choice of cathode material is also critical as was seen from the varying responses of the ion distributions to a magnetic field, for the different materials.

We intend to pursue some open questions form this paper, such as if our estimate of the effective cathode radius is realistic and how the ion flux is really distributed for the annular geometry. The experiment can be made more coherent by measuring the thrust directly as a basis for comparison to the value derived by computation, as well as refining the Faraday cup measurements for direct measurement of ion current.

CRediT authorship contribution statement

T. Rencken: Investigation. **P. Ferrer:** Supervision.

Declaration of competing interest

The authors declare that they have no known competing financial interests or personal relationships that could have appeared to influence the work reported in this paper.

References

[1] Marsil AC. Silva, et al., A review of MEMS micropropulsion technologies for CubeSats and PocketQubes, Acta Astronaut. 143 (2018) 234–243.

[2] B. Larangot, et al., "Solid propellant microthruster: an alternative propulsion device for nanosatellite." Aerospace Energetic Equipment Conference (Avignon, France) 40 (5) (2002).

[3] C.P. Hiemstra, Design, Production, and Validation of a Vacuum Arc Thruster for In-Orbit Proximity Operations, Dissertation, 2022.

[4] James E. Polk, et al., A theoretical analysis of vacuum arc thruster and vacuum arc ion thruster performance, IEEE Trans. Plasma Sci. 36 (5) (2008) 2167–2179.

[5] S. Bai, et al., Performance model of vacuum arc thruster with inductive energy storage circuit, Acta Astronaut. 186 (2021) 426–437, https://doi.org/10.1016/J.ACTAASTRO.2021.06.008. ISSN: 0094-5765.

[6] M. Kühn, C. Toursel, J. Schein, Thrust measurements on the high efficient and reliable Vacuum Arc Thruster (HERVAT), Appl. Sci. 11 (5) (2021) 2274, https://doi.org/10.3390/app11052274.

[7] M. Kühn, J. Schein, Development of a high-reliability Vacuum Arc Thruster system, J. Propul. Power 38 (5) (2022) 752–758.

[8] Michael Keidar, et al., Magnetically enhanced vacuum arc thruster, Plasma Sources Sci. Technol. 14 (4) (2005) 661.

[9] Igal Kronhaus, Satyajit Chowdhury, Matteo Laterza, Axial Magnetic Field Effect on Vacuum Arc Thruster Performance, arXiv preprint arXiv:1912, 2019 11657.

[10] Denis B. Zolotukhin, et al., Demonstration of electric micropropulsion multimodality, Sci. Adv. 8 (2022) eadc9850, https://doi.org/10.1126/sciadv.adc9850.

[11] Qimeng Xia, et al., The influence of external magnetic field on the plume of vacuum arc thruster, Acta Astronaut. 164 (2019) 69–76.

[12] Lijun Wang, et al., Research progress of model of vacuum arc and anode activity under axial magnetic fields, IEEE Trans. Plasma Sci. 47 (8) (2019) 3496–3507.

[13] Hang Li, et al., A model for macro-performances applied to low power coaxial pulsed plasma thrusters, Acta Astronaut. 170 (2020) 154–162.

[14] Oleg O. Baranov, Uroš Cvelbar, Kateryna Bazaka, Concept of a magnetically enhanced vacuum arc thruster with controlled distribution of ion flux, IEEE Trans. Plasma Sci. 46 (2) (2017) 304–310.

[15] Kazunori Takahashi, et al., Effect of magnetic and physical nozzles on plasma thruster performance, Plasma Sources Sci. Technol. 23 (4) (2014) 044004.

[16] J. Kutzner, H.C. Miller, Ion flux from the cathode region of a Vacuum Arc, IEEE Trans. Plasma Sci. 17 (5) (1989) 688–694.

[17] J.E. Daalder, Components of cathode erosion in vacuum arcs, J. Phys. Appl. Phys. 9 (16) (1976) 2379.

[18] C.W. Kimblin, Cathode spot erosion and ionization phenomena in the transition from vacuum to atmospheric pressure arcs, J. Appl. Phys. 45 (12) (1974) 5235–5244.

[19] G. Yushkov, A. Anders, E. Oks, I. Brown, Ion velocities in Vacuum Arc plasmas, J. Appl. Phys. 88 (10) (2000) 5618–5622.

[20] Isak I. Beilis, M.P. Zektser, Calculation of the parameters of the cathode stream of an arc discharge, High Temp. 29 (1991) 501–504.

[21] D. Zolotukhin, et al., Discharge characteristics of two-stage micro-cathode arc MPD thrusters with a permanent magnet and a pulsed magnetic field, J. Phys. D Appl. Phys. 54 (2021) 015201.

[22] Lun Jonathan, Performance improvement of vacuum arc thrusters. Diss. University of the Witwatersrand, Faculty of Engineering and the Built Environment, School of Mechanical, Industrial & Aeronautical Engineering (2015).

[23] Mary Anne White, Physical Properties of Materials, CRC press, 2018, p. 496. ISBN: 9781138605107.

[24] Satyajit Chowdhury, Igal Kronhaus, "Characterization of vacuum arc thruster performance in weak magnetic nozzle.", Aerospace 7 (6) (2020) 82.